DOI: 10.61782/fa.2025.0789

FORUM ACUSTICUM
EURONOISE 2025

SOUND SOURCE DIRECTIVITY ESTIMATION VIA A SPHERICAL WAVE DECOMPOSITION OF THE RADIATED FIELD: APPLICATION TO HUMAN VOICE DIRECTIVITY MEASUREMENTS

Matthieu Hartenstein[1*] **Paul Luizard**[3,4] **Hélène Moingeon**[2]
Cédric Pinhède[2] **Marc Pachebat**[2] **Christian Ollivon**[1]
François Ollivier[1] **Fabrice Silva**[2]

[1] Institut Jean le Rond ∂'Alembert, Sorbonne Université, CNRS UMR 7190, Paris, France
[2] Aix Marseille Université, CNRS, Centrale Méditerranée, LMA UMR 7031, Marseille, France
[3] Univ. Grenoble Alpes, CNRS, Grenoble INP, GIPSA-lab, Grenoble, France
[4] Audio Communication Group, Technische Universität Berlin, Germany

ABSTRACT

The experimental evaluation of the directivity of a non-repeatable sound source necessitates the simultaneous acquisition of signals from microphones distributed on a sphere centered on the source with a high spatial resolution. Placing a high number of microphones at precise, pre-determined positions is a laborious task that is subject to inaccuracies. The Helmholtz Equation Least Squares (HELS) method is an imaging technique originally used in near-field acoustic holography. This method involves decomposing the sound field measured around a source into a basis of functions that solve the Helmholtz equation. Once this decomposition has been identified, any acoustic quantity can be reconstructed around the source. Recent simulated and experimental studies have demonstrated that the HELS method consistently estimates the far-field directivity of a sound source from measurements performed on an arbitrary surface around the source. The present study utilizes a sphere-like array of 3 m-diameter and around 600 MEMS microphones installed in an anechoical room to measure the directivity of a reference sound source. The truncation order of the basis function is chosen based on a cross-validation procedure and on stability considerations. Measurements on human singers are presented and compared to recent findings on human voice directivity.

Keywords: Directivity reconstruction, surrounding microphone arrays, spherical waves.

**Corresponding author*: matthieu.hartenstein@sorbonne-universite.fr.

1. INTRODUCTION

Over the past two decades, numerous research projects have investigated the directivity of natural sound sources [1, 2], particularly that of the human voice [3–5]. Indeed, the latter can present complex patterns due to the geometric peculiarities of the face and body of the speaker [3]. Most of these works are affected by some of the following limitations. Firstly the estimates may be restricted to horizontal and/or vertical planes [3] failing to account for the inherently 3D nature of vocal radiation. Going beyond 2D planes has been attained by either scanning a surrounding sphere by moving an array of microphones around the speaker [4], or paving the sphere with a rather low number of microphones [5]. Both options have major drawbacks. The former relies on the strong assumption that vocalisations are repeatable enough to ensure a reliable 3D reconstruction, while the latter requires the use of interpolation methods to enhance the resolution of the directivity function estimate [5].

The Helmholtz Equation Least Squares (HELS) method was introduced in order to reconstruct the acoustic quantities on a vibrating surface of arbitrary shape [6].

It relies on the expansion of the acoustic field around the source in an orthonormal basis of functions that satisfy the wave equation. In spherical coordinates, this is known as the spherical wave decomposition (SWD).

Despite its initial development for near-field acoustic holography (NAH), the HELS method has recently been applied to the far-field directivity (FFD) estimation of sound sources in numerical and real-life experiments involving hundreds of microphones [1,7,8]. However, the existing experimental studies focus on controlled sources and only barely address the definition of an adequate truncation order N for the SWD. Ref. [8] proposes to choose a value of N that minimizes a cross-validation metric, but does not analyse the behaviour of this metric with N.

In this work, the HELS method is first applied to the experimental reconstruction of the FFD of human voice. Section 2 recalls the principle of the HELS method and presents the experimental setup used in the present study. Section 3 analyses the behaviour of the cross-validation error defined in Ref. [8] and proposes a mixed criterion that accounts for both the cross-validation error and the stability of the HELS inverse problem for defining an optimal truncation order. Section 4 shows that the measurements on the controlled source highlight the order limitation of the array, and presents examples of reconstructed human voice FFD. Section 5 concludes the present study.

2. METHOD

2.1 The HELS method for far-field directivity estimation

2.1.1 *Formulation of the HELS inverse problem*

At frequency f and corresponding acoustic wavenumber $k = 2\pi f/c_0$ (with c_0 the speed of sound in air), the sound field radiated by a sound source centered at the origin of a system of spherical coordinates (r, θ, ϕ) can be expanded as a weighted sum of spherical waves $(\psi_n^m(kr, \theta, \phi))_{(n\in\mathbb{N}, m\leq n)}$ [9]

$$p(r, \theta, \phi) = \sum_{n=0}^{+\infty} c_{mn}(k)\psi_n^m(kr, \theta, \phi), \tag{1}$$

where $c_{mn}(k)$ are the coefficients of the expansion. The spherical waves of order n and degree m are products of a spherical Hankel functions $h_n(kr)$ of the second kind and of spherical harmonic functions of order n and degree m.

If the sound field is sampled around the source at Q positions $(r_q, \theta_q, \phi_q)_{q\in[0,\dots,Q-1]}$ and if the series in Eq. (1) is truncated at order N, the vector $\mathbf{p}$ of measured pressures $(p(r_q, \theta_q, \phi_q))_{q\in[0,\dots,Q-1]}$ can be written [7]

$$\mathbf{p} = \mathbf{H}\mathbf{c}, \tag{2}$$

where $\mathbf{c}$ is the truncated vector of the $(N+1)^2$ coefficients $(c_{mn}(k))$ arranged in a column according to the Ambisonic Number Sequence, and where $\mathbf{H}$ is a matrix whose columns correspond to spherical waves of given orders and degrees sampled at the measurement positions.

2.1.2 *Estimation of the far-field directivity function*

The vector of the truncated SWD coefficients (2) can be estimated in a ℓ_2-regularized least-squares fashion

$$\hat{\mathbf{c}} = (\mathbf{H}^H\mathbf{H} + \lambda\mathbf{I})^{-1}\mathbf{H}^H\mathbf{p}, \tag{3}$$

where H is the Hermitian transposition, $\mathbf{I}$ is the $(N+1)^2 \times (N+1)^2$ identity matrix, and λ is a regularization coefficient. Ref. [1] mentions that regularization improves the reconstruction when the array used for the measurement presents uncovered areas. The array shown in Fig. 1 is supposed sufficiently dense, which justifies the absence of regularization in what follows ($\lambda = 0$).

The acoustic pressure can be estimated anywhere around the source using the SWD in Eq. (1) and the vector $\hat{\mathbf{c}}$ of estimated spherical wave coefficients $(\hat{c}_{mn})$. Furthermore, the far-field directivity of the source can be reconstructed using the following formula [2]

$$D_\infty(\theta, \phi) = \sum_{n=0}^{N}\sum_{m=-n}^{n} \hat{c}_{mn} j^{(n+1)} Y_n(\theta, \phi). \tag{4}$$

2.1.3 *Cross-validation procedure*

In Refs. [1,4], the choice of a SWD truncation order N is done by hand. Ref. [7] proposes a method based on a far-field assumption in order to mitigate the instability of the inverse problem in Eq. (2) when high-order components are included in the spherical wave basis. In practice, this method is limited to the lower frequency range where source-sensor distances are small behind the wavelength.

Ref. [8] proposes to use a cross-validation framework that allows to define the truncation order optimally. The set $\mathcal{E}$ of microphones is partitioned into S random disjoint validation subsets $(\mathcal{E}_s)_{s\in[0,\dots,S-1]}$. For each validation subset $\mathcal{E}_s$, the HELS method is used to estimate a vector of SWD coefficients $\hat{c}_s$ given measurement data in the complement set of points $\mathcal{E} - \mathcal{E}_s$. The pressure is then reconstructed on the validation points in $\mathcal{E}_s$ using the

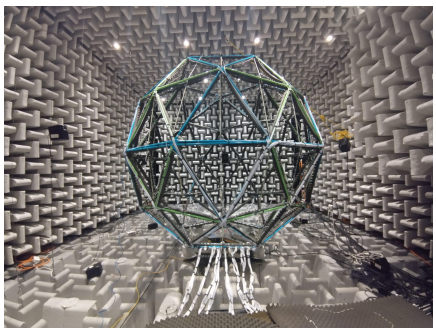

Figure 1: Microphone array used in the study.

coefficients $\hat{c}_s$. The partitioning of $\mathcal{E}$ into disjoint validation subsets ensures that an unique estimate $\hat{p}(r_q, \theta_q, \phi_q)$ is available for each measurement point (r_q, θ_q, ϕ_q). A RMS cross-validation error relative to the RMS pressure measured on the array can then be computed

$$\mathcal{L}_{\text{CV}} = \frac{\sqrt{\sum_{q=0}^{Q-1} |p(r_q, \theta_q, \phi_q) - \hat{p}(r_q, \theta_q, \phi_q)|^2}}{\sqrt{\sum_{q=0}^{Q-1} |p(r_q, \theta_q, \phi_q)|^2}}. \quad (5)$$

2.2 Experimental setup

2.2.1 Microphone array

The 3.6 m-radius quasi-spherical array of 588 microphones shown in Fig. 1 is deployed in the anechoic chamber of Laboratoire de Mécanique et d'Acoustique (Marseille, France). The microphone positions are retrieved using the procedure described in Ref. [10].

2.2.2 Measurements on a reference controlled source

For validation purposes, measurements are first performed on a controlled source. The sound source used in the experiment is a 3.5 cm-radius speaker mounted on a 8.5 cm 3D-printed spherical baffle. This sound source is assumed to present similar directivity characteristics as a spherical cap of aperture 4 cm on a rigid baffle of radius 8.5 cm. The field radiated by the spherical cap admits an analytical spherical wave decomposition (see *e.g.* Ref. [9]), which allows to compute reference fields for a qualitative comparison with the fields reconstructed in the experiment.

The signal sent to the source is a Synchronized Swept Sine [11] of duration 30 s spanning the frequency range 100 Hz to 10 000 Hz. The Megamicros acquisition system described in Ref. [12] is used to acquire the signals measured by the array, with a sampling frequency of 50 kHz. The procedure from Ref. [11] is used to isolate the linear component of the source's frequency response recorded by each microphone. These responses are normalized by the linear response measured by a frontal microphone. At a given frequency, the normalized linear response are used to construct the input vector in the HELS method.

2.2.3 Singer recordings

First applications of the HELS method to the reconstruction of the directivity of human voice are performed. An amateur singer is asked to utter the French vowel /a/, singing a glissando of 30 s spanning approximately two octaves. The singer is asked to keep their mouth approximately at the center of the sphere, and their posture is visually controlled during the utterance using a camera.

Power and cross spectral densities of the signals recorded by the MEMS microphones are computed using Welch's method [13] with a 20 ms long Hann window and 80 % overlap. Transfer functions between the reference MEMS microphone placed directly in front of the speaker and the remaining MEMS microphones are used as inputs for the HELS method.

3. CHOICE OF A TRUNCATION ORDER

3.1 Evolution of the cross-validation error with N

Figure 2 shows the evolution of the cross-validation error $\mathcal{L}_{\text{CV}}$ with the truncation order at three different frequencies, for the controlled source and the singer. At all frequencies, $\mathcal{L}_{\text{CV}}$ is high at low orders and starts by decreasing to reach a low error plateau. At a mid-range frequency of 500 Hz, it keeps decreasing at a low rate on the whole range of truncation order represented, presenting a minimal value at $N = 12$ for both sources. At 2 kHz, $\mathcal{L}_{\text{CV}}$ slightly increases at higher orders for both sources, presenting a global minimum (5 for the controlled source, $9 - 11$ for the singer). At 4 kHz, the cross-validation error for the controlled source is minimal at $9 - 10$, while the cross-validation error for the singer does not reach its minimal value before $N = 12$.

3.2 Condition number of the inverse problem

The condition number $\kappa = ||\mathbf{H}||_2 ||\mathbf{H}^{-1}||_2$ (where $||.||_2$ is the ℓ_2 matrix norm) of a matrix $\mathbf{H}$ gives an indication of the well-posedness of the associated inverse problem [14]. High condition numbers are associated to unstable systems with a low robustness to uncertainties. Figure 3 shows the evolution of the condition number of the HELS

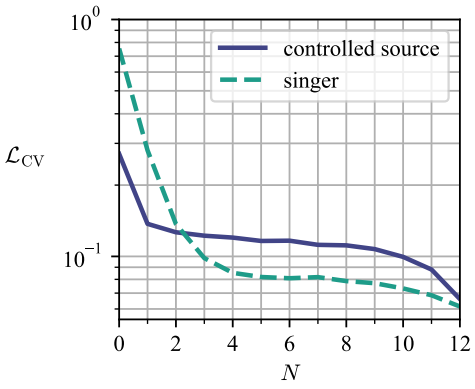

(a) 500 Hz

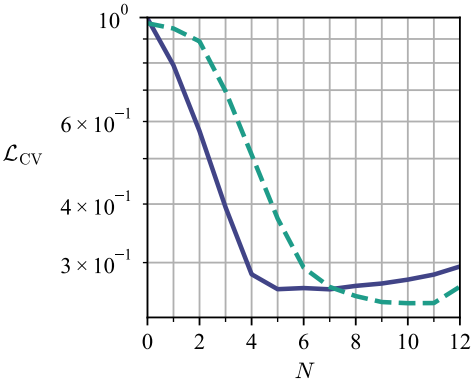

(b) 2 kHz

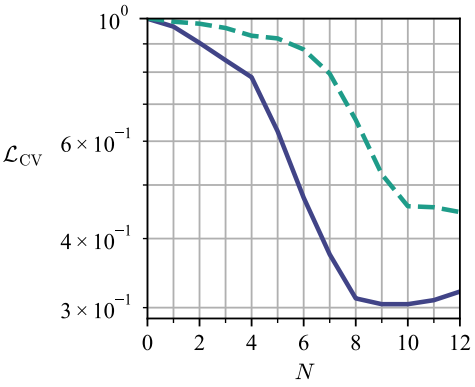

(c) 4 kHz

Figure 2: Evolution of the cross-validation error with the truncation order at three different frequencies, for the controlled source and the singer.

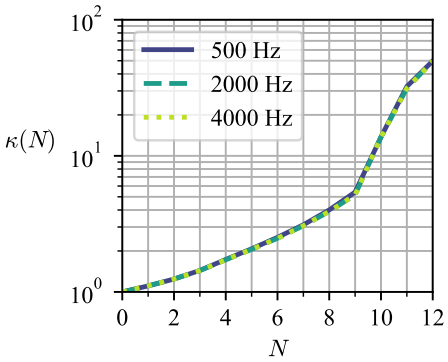

Figure 3: Evolution of the condition number κ of the sensing matrix $\mathbf{H}$ with the truncation number N at 500 Hz (solid purple curve), and 2 (dashed blue curve) and 4 kHz (dotted green curve).

problem's sensing matrix $\mathbf{H}$ with the truncation order N at 500 Hz, 2 kHz, and 4 kHz. At all the considered frequencies, the condition number curves are close to identical. The condition number monotonically increase with N. At orders higher than 9, the condition number it a higher increase rate than at lower orders. Therefore, using truncation orders higher than 10 might lead to an unstable inversion of Eq. (2).

3.3 Choice of an optimal truncation order

In order to ensure the well-posedness of the inverse problem in Eq. (2) and to improve the robustness of the HELS method to experimental uncertainties, the truncation order is chosen in terms of both the cross-validation error and the condition number κ. First of all, the truncation order is sought for in the range where the condition number has not started to critically increase, which corresponds to the range $I = [0, \ldots, 9]$ in the present study case. At a given frequency, we propose to define the optimal truncation order as the one which yields the lowest condition number κ under the constraint that the cross-validation error is close enough to the minimal achievable cross-validation error $\mathcal{L}_{\text{min}} = \arg\min_{N \in I} \mathcal{L}_{\text{CV}}(N)$. This can be stated as

$$\begin{aligned} N_{opt} &= \arg\min_{N \in I} \kappa(N) \\ \text{s.t. } &|\mathcal{L}_{\text{CV}}(N) - \mathcal{L}_{\text{min}}| \leq \epsilon, \end{aligned} \tag{6}$$

where ϵ is the maximal acceptable distance to the minimal error. In the remaining of this study, $\epsilon = 0.01$.

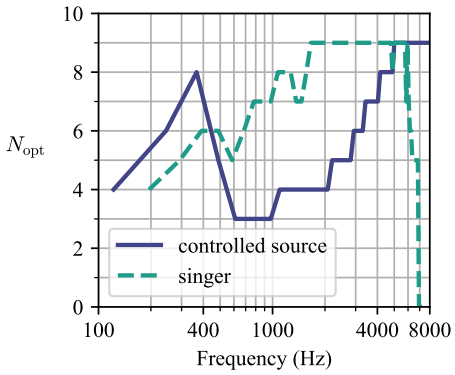

Figure 4: Frequency evolution of the optimal truncation order defined in Eq. (6) for the measurements on the controlled source and on the singer.

3.4 Evolution of N_{opt} with frequency

Figure 4 shows the frequency evolution of the optimal truncation order with frequency for the two sources of interest. For the singer, a truncation order $N = 4$ is obtained at 200 Hz, and the truncation order presents an increasing trend with increasing frequency up to approximately 2 kHz, where it reaches the maximal order $N = 9$. At very high frequency above 6 kHz, the optimal truncation order for the singer drops. This is likely due to the HELS method being too restricted in order to reproduce the complexity of the sound field. In the 100 Hz to 600 Hz frequency range, the optimal truncation order for the controlled source is critically high (approximately 6 to 7). This indicates a high complexity of the radiated field in this frequency range. This complexity can be explained by a coupling between the air volume inside the spherical baffle and the tube used to connect the source to its support, despite efforts to dampen the resonance of the mast filling it with foam, and to reduce the acoustic leaks. At frequency higher than 600 Hz, the optimal truncation order for the controlled source drops to 3, and increases monotonically with frequency, reaching $N = 9$ at 5 kHz. In this same frequency range, the optimal truncation order obtained for the controlled source is lower than the one obtained for the singer, indicating a higher complexity of the field radiated by the singer.

4. RECONSTRUCTED FIELDS

4.1 Controlled source : Visualization of the array's order limitation

Figure 5 (a) shows the theoretical FFD of the spherical cap source model at 500 Hz. At such a low frequency, a wide main lobe is observed in front of the source, and the FFD function presents a rear lobe approximately 1 dB lower than the frontal lobe.

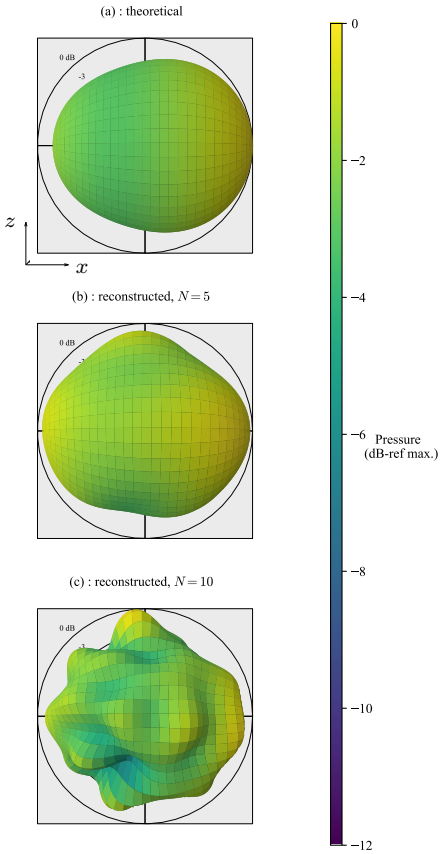

Figure 5: (a) : Magnitude of the theoretical 500 Hz FFD function of the spherical cap. (b), (c) : magnitude of the 500 Hz FFD reconstructed experimentally for the controlled source with the HELS method, using truncation orders of 5 and 10. In a particular direction, the color and distance to the origin indicate the radiated power. The x and z axis indicated in (a) correspond to the frontal and upward directions.

The reconstruction of the controlled source's FFD at 500 Hz using respective truncation orders of 5 and 10 are shown in Figs. 5 (b) and (c). The FFD reconstruction using $N = 5$ presents similar frontal and rear lobes as the theoretical FFD, and an upper lobe of similar amplitude as the rear lobe. This upper lobe might result from the diffraction of the source's support. The reconstruction using the truncation order $N = 10$ presents high rate spatial fluctuation that are unlikely to be radiated in the far-field considering the large wavelength (approximately 69 cm) at this low frequency. These fluctuations are likely due to the experimental uncertainties impacting the reconstruction at a truncation order where the condition number is relatively high, motivating the use of a truncation order lower or equal to 9.

4.2 Reconstructed human voice directivity

4.2.1 Horizontal plane

Figure 6 (a) shows the frequency evolution of the singer's reconstructed FFD in the horizontal plane. Below 600 Hz, the horizontal directivity presents a wide frontal lobe. On the entire frequency range, the FFD function in the horizontal plane presents a rear lobe of decreasing radiated power and angular width with increasing frequency. At frequency higher than 500 Hz, strong side lobes appear in the FFD function. These side lobes tend to decrease in terms of both width and radiated power, and to diverge from the center with increasing frequency. New side lobes with a similar behaviour appear at around 1.5 kHz. In the frequency ranges 600 Hz to 900 Hz and 1500 Hz to 2000 Hz, the side lobes have a higher amplitude than the frontal lobe, and the main radiation direction in the horizontal plane is not frontal. In the respective ranges 1000 Hz to 1500 Hz and 2000 Hz to 4500 Hz, the main radiation direction in the horizontal plane is frontal again. Furthermore, the frontal lobe's width in the range 1000 Hz to 1500 Hz is narrower than in the range 200 Hz to 600 Hz and wider than in the range 2000 Hz to 4500 Hz.

In Ref. [3], Brandner *et al.* measure the directivity of a classical singer asked to sing a glissando on the German vowel /a/ using an horizontal and a vertical arc of microphones of angular resolution 11.25°. The main characteristics of the FFD function in the horizontal plane seen in Figure 6 (a) and mentioned in the last paragraph (frontal maximum radiation direction at most frequency, presence of diverging and narrowing side lobes, maximum radiation direction on the sides in some frequency regions, decaying and narrowing rear lobe) can be observed in their

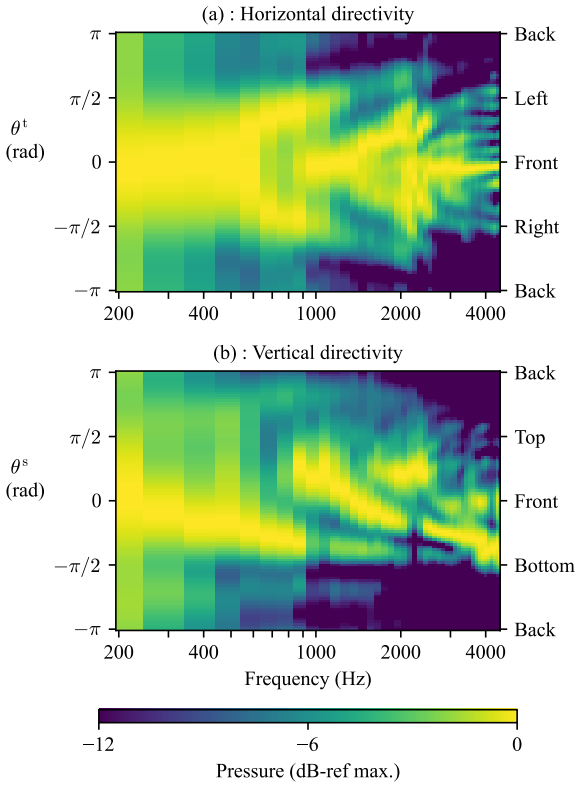

Figure 6: Frequency-angle representations of the reconstructed singer's FFD function in the horizontal (a) and sagittal (b) planes. The FFD function is normalized by the maximal value at each frequency.

results (Figs. 13 (a) and (c) in the corresponding study). However, from about 3 kHz, the FFD function in the horizontal plane shown in Figure 6 (a) presents unexpected narrow lobes of constant angles with varying frequency. At this frequency, the optimal truncation order for the singer (see Fig. 4) has reached $N = 9$, while the spatial complexity of the radiated field is likely to increase. This result highlights the need for microphone arrays of very high orders when studying complex sound sources such as human singers or musical instruments in the high frequency range.

4.2.2 Sagittal plane

Figure 6 (b) shows the frequency evolution of the singer's reconstructed FFD in the horizontal plane. At very low frequency (200 Hz), a strong lobe appears in front (sagittal

angle $\theta_s = 0\,\mathrm{rad}$) of the source. At respectively approximately $800\,\mathrm{Hz}$ and $1500\,\mathrm{Hz}$, the FFD function in the vertical direction presents upward-directed lobes ($\theta_s \approx \pi/4$ rad). The directions and widths of these lobes decrease with frequency. A striking consequence of these observations, also observed in the measurements by Brandner *et al.* [3], is that the main radiation direction in the vertical plane is horizontal only at some isolated frequencies.

This last result is the topic of a study by Pörschmann *et al.* [15], who estimate the vertical maximum radiation direction of the field radiated by human speakers using an order 4 surrounding spherical array of microphones. Note that the resolution of the FFDs shown in Ref. [15] (Fig. 1 and 2) is not sufficient to observe all the characteristics mentioned in the last paragraph, motivating again the need for very high arrays of microphones when analyzing the directivity of natural sources.

4.2.3 Examples of 3D directivities

Figure 7 shows balloon plots of the reconstructed singer's FFD function at three different frequencies. At a midrange frequency of $500\,\mathrm{Hz}$ (Figure 7 (a)), the FFD presents a downward-directed frontal main lobe, a weaker upward-directed rear lobe, and a third downward-directed rear lobe. At higher frequencies (1.9 and $2.3\,\mathrm{kHz}$ in Figure 7 (b) and (c)), the FFD function presents secondary lobes that are neither contained in the horizontal or in the vertical plane. This illustrates the limitation of studying the directivity of sound sources by performing 2D measurements.

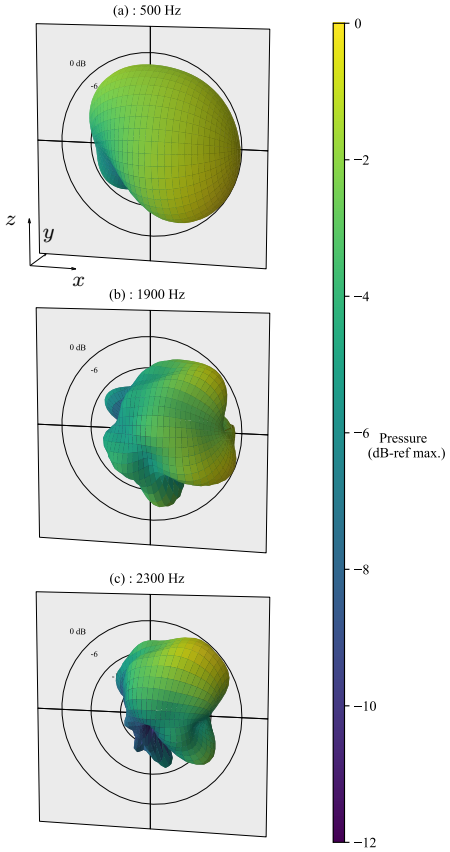

Figure 7: 3D representations of the magnitude of the reconstructed singer's FFD at three different frequencies. In a particular direction, the distance to the origin indicates the radiated power. To ease readability, a color scale is added to the representation, and iso-power circles are added to the representation. The x (resp. y, z) axis indicated in (a) correspond to the frontal (resp. left, upward) direction. The FFD is normalized by its maximal value at each frequency.

5. CONCLUSIONS

This work presented an experimental validation of the HELS method used for the directivity reconstruction of sound sources. A criterion was proposed to choose an optimal truncation order for the spherical wave decomposition of the sound field based on considerations on both a cross-validation error metric and on the condition number of the HELS inverse problem.

A quasi-spherical array of approximately 600 microphones and diameter $3.6\,\mathrm{m}$ was used to measure the field radiated by a reference controlled source and a human singer. At midrange frequency (below $600\,\mathrm{Hz}$), the high spatial complexity of the controlled source put into light the order limitation of the array. At higher frequency, the optimal truncation order for the controlled source was lower than the one obtained for the singer. This is in accordance with the expected higher spatial complexity of

the sound field radiated by the singer.

The reconstructed FFD function of the human singer presented a hardly explainable behaviour at high frequency (above approximately 2.5 kHz) where the optimal truncation order is higher than 9. To the knowledge of the author, the maximal spherical harmonic order of the synchronous spherical arrays typically used in the literature for directivity interpolation is 4 to 5 (see, *e.g.*, Ref. [15]). This observation demonstrates the resolution limitation of previously published studies at high frequency. Finally, 2D and 3D examples of reconstructed directivity for the singer presented a good agreement with recently published results on human voice directivity, which were either limited to the horizontal and vertical plane, or performed with a lower order spherical array.

6. ACKNOWLEDGMENTS

This work is funded by the French National Research Agency (ANR-21-CE42-0017,2021-25) as part of the Rayovox project.

7. REFERENCES

[1] S. D. Bellows and T. W. Leishman, "Obtaining far-field spherical directivities of guitar amplifiers from arbitrarily shaped arrays using the Helmholtz equation least-squares method," in *Proc. Mtgs. Acoust.*, vol. 42, (held online), Dec. 2020.

[2] J. Ahrens and S. Bilbao, "Computation of Spherical Harmonic Representations of Source Directivity Based on the Finite-Distance Signature," *IEEE/ACM Transactions on Audio, Speech, and Language Processing*, vol. 29, pp. 83–92, 2021.

[3] M. Brandner, R. Blandin, M. Frank, and A. Sontacchi, "A pilot study on the influence of mouth configuration and torso on singing voice directivity," *The Journal of the Acoustical Society of America*, vol. 148, pp. 1169–1180, Sept. 2020.

[4] T. W. Leishman, S. D. Bellows, and C. M. Pincock, "High-resolution spherical directivity of live speech from amultiple-capture transfer function method," *The Journal of the Acoustical Society of America*, vol. 149, no. 3, p. 18, 2021.

[5] C. Pörschmann and J. M. Arend, "Investigating phoneme-dependencies of spherical voice directivity patterns," *The Journal of the Acoustical Society of America*, vol. 149, pp. 4553–4564, June 2021.

[6] Z. Wang and S. F. Wu, "Helmholtz equation–least-squares method for reconstructing the acoustic pressure field," *The Journal of the Acoustical Society of America*, vol. 102, pp. 2020–2032, Oct. 1997.

[7] M. Hartenstein, P. Luizard, H. Moingeon, C. Pinhède, M. Pachebat, C. Ollivon, F. Ollivier, and F. Silva, "A Method for Directivity Estimation with a High-Order Non-Spherical Microphone Array," in *Proc. Forum Acusticum*, (Torino, Italy), 2023.

[8] M. Hartenstein, F. Ollivier, H. Moingeon, M. Meinnel, C. Ollivon, A. Sokpoli, M. Pachebat, C. Pinhède, F. Silva, and P. Luizard, "Far-field directivity estimation with a cube-shaped array of 256 MEMS microphones," in *Proc. Internoise*, (Nantes, France), 2024.

[9] E. G. Williams, *Fourier Acoustics*. London: Academic press, 1999.

[10] M. Hartenstein, P. Luizard, H. Moingeon, C. Pinhède, C. Ollivon, F. Ollivier, F. Silva, and M. Pachebat, "Enhancing the geometrical calibration of microphones arrays : solutions and experimental validation," in *Proc. Forum Acusticum*, (Malaga, Spain), 2025.

[11] A. Novak, P. Lotton, and L. Simon, "Synchronized Swept-Sine: Theory, Application, and Implementation," *Journal of the Audio Engineering Society*, vol. 63, pp. 786–798, Nov. 2015.

[12] C. Vanwynsberghe, *Réseaux à grand nombre de microphones : applicabilité et mise en oeuvre*. PhD thesis, Université Pierre et Marie Curie, Paris, France, Sorbonne Université, Paris, France, 2016.

[13] P. Welch, "The use of fast Fourier transform for the estimation of power spectra: A method based on time averaging over short, modified periodograms," *IEEE Transactions on Audio and Electroacoustics*, vol. 15, pp. 70–73, June 1967.

[14] P. C. Hansen, *Discrete Inverse Problems: Insight and Algorithms*, vol. 7 of *Fundamentals of Algorithms*. Philadelphia: Society for Industrial and Applied Mathematics, 2010.

[15] C. Pörschmann and J. M. Arend, "On the impact of downward-directed human voice radiation on ground reflections," *Acta Acustica*, vol. 8, p. 12, 2024.